Seasonal dynamics of sea surface salinity off Panama: The far Eastern Pacific Fresh Pool

Gaël Alory,[1] Christophe Maes,[2] Thierry Delcroix,[2] Nicolas Reul,[3] and Serena Illig[2,4]

[1]   The freshest surface waters in the tropical Pacific are found at its eastern boundary. Using in situ observations, we depict the quasi-permanent presence of a far eastern Pacific fresh pool with sea surface salinity (SSS) lower than 33, which is confined between Panama's west coast and 85°W in December and extends westward to 95°W in April. Strong SSS fronts are found at the outer edge of this fresh pool. We investigate the seasonal dynamics of the fresh pool using complementary satellite wind, rain, sea level and in situ oceanic current data at the surface, along with hydrographic profiles. The fresh pool appears off Panama due to the strong summer rains associated with the northward migration of the ITCZ over Central America in June. During the second half of the year, the eastward-flowing North Equatorial Counter-Current keeps it trapped to the coast and strengthens the SSS front on its western edge. During winter, as the ITCZ moves southward, the northeasterly Panama gap wind creates a southwestward jet-like current in its path with a dipole of Ekman pumping/eddies on its flanks. As a result, upwelling in the Panama Bight brings to the surface cold and salty waters which erode the fresh pool on its eastern side while both the jet current and the enhanced South Equatorial Current stretch the fresh pool westward until it nearly disappears in May. New SMOS satellite SSS data proves able to capture the main seasonal features of the fresh pool and monitor its spatial extent.

Citation: Alory, G., C. Maes, T. Delcroix, N. Reul, and S. Illig (2012), Seasonal dynamics of sea surface salinity off Panama: The far Eastern Pacific Fresh Pool, *J. Geophys. Res.*, *117*, C04028, doi:10.1029/2011JC007802.

1. Introduction

[2] The eastern tropical Pacific Ocean between about 120°W and South America is unique in many respects. Lying in an environment predominantly influenced by the South and North-Eastern trades and the doldrums, and seasonally affected by the winds from the Caribbean, this region is characterized by a complicated surface circulation and large seasonal variations in wind, current, temperature and salinity. Moreover, seasonal and longer timescales as associated with the El Niño–Southern Oscillation (ENSO) variability are typically of similar amplitude [*Fiedler and Talley*, 2006]. This physical environment supports large and relatively unique biological communities from plankton to tuna, marine mammals and seabirds [*Schaefer and Fuller*, 2002; *Pennington et al.*, 2006; *Ballance et al.*, 2006], including coral reefs [*Glynn et al.*, 2001].

[3] The eastern tropical Pacific is composed of two main regions that are dynamically and ecologically different: the eastern Pacific warm pool and the equatorial cold tongue. The eastern Pacific warm pool, characterized by a mean sea surface temperature (SST) greater than 28°C and centered around 15°N along the coast of Central America (Figure 1), is a region of strong ocean-atmosphere interactions [*Xie et al.*, 2005]. Besides, the equatorial cold tongue with a mean SST of 24°C has been recognized as a major feature of the upwelling system at both seasonal and interannual timescales [*Wyrtki*, 1981; *Wang*, 1994; *Kug et al.*, 2009]. Between these two main regions, the atmospheric Inter-tropical Convergence Zone (ITCZ) is closely associated with the eastern termination of the equatorial current system and, as it meets the Central American topography, generates strong winds driving smaller-scale patterns such as the Costa Rica dome [*Kessler*, 2006, and references therein].

[4] The lowest sea surface salinity (SSS) of the tropical Pacific is found between the warm pool and the cold tongue regions, with SSS values lower than 33 off the Panama isthmus and SSS values lower than 34 extending as far as 130°W from the equator to 15°N (Figure 1). Note that salinity computations are based on the Practical Salinity Scale PSS-78, and reported with no units [*United Nations Educational, Scientific and Cultural Organization*, 1981]. Using the term coined for the western Pacific [*Delcroix and Picaut*, 1998; *Hénin et al.*, 1998], we can define the region with SSS lower than 34 as the Eastern Pacific Fresh Pool (EPFP) and its core where SSS is in permanence lower than 33 as the far EPFP. These low salinity regions were already described by *Bennett* [1966], to the author's knowledge from

[1]LEGOS, OMP, CNAP, Université de Toulouse, Toulouse, France.
[2]LEGOS, IRD, Université de Toulouse, Toulouse, France.
[3]LOS, IFREMER, Plouzané, France.
[4]IMARPE, Callao, Peru.
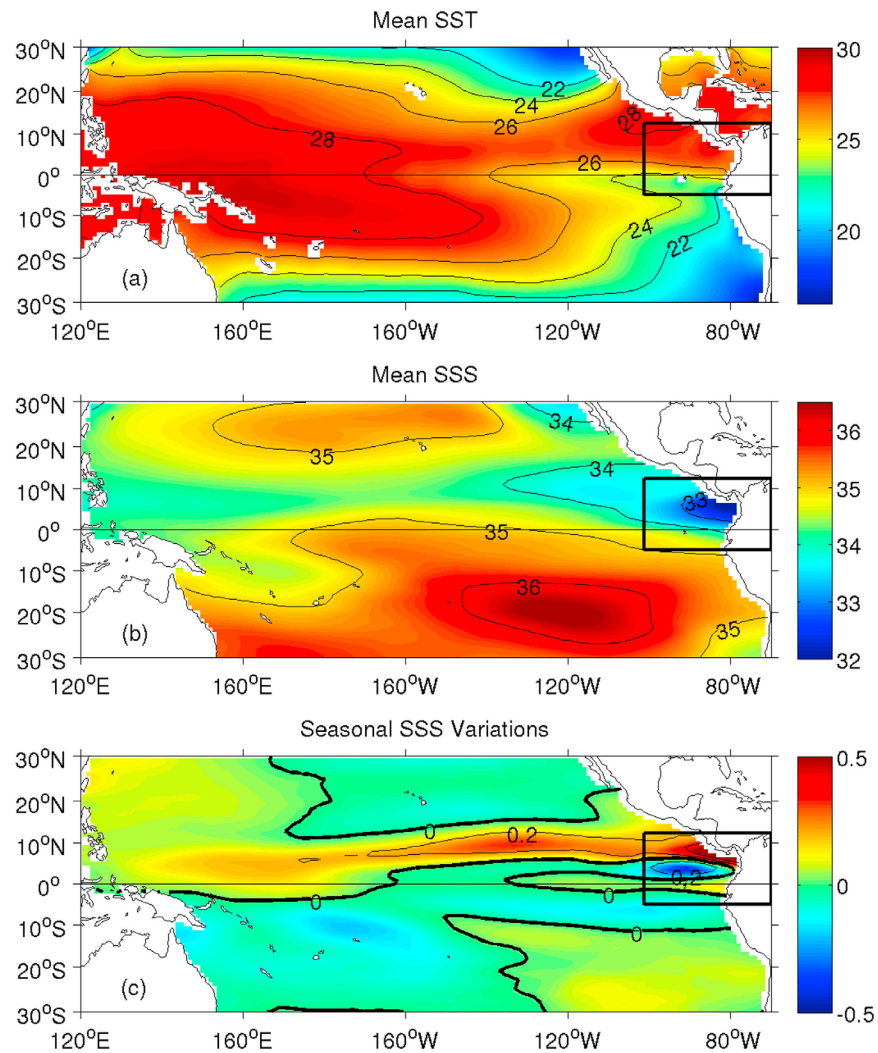
Figure 1. Mean (a) SST (°C), (b) SSS and (c) first seasonal EOF of SSS in the tropical Pacific Ocean. Seasonal values correspond to peak anomalies in March; opposite anomalies are found in October. The eastern box delimits our region of study.

the first climatological SSS charts of the eastern Pacific. Compared to its western counterpart [e.g., *Cravatte et al.*, 2009], the EPFP limit is easier to define by a single isohaline value; it also partially overlaps with the Eastern Pacific Warm Pool. The EPFP reflects both the conditions of excess precipitation over evaporation beneath the ITCZ and inputs of freshwater from the Andes and Caribbean region [*Benway and Mix*, 2004]. Analysis of a recent gridded SSS product [*Delcroix et al.*, 2011] points out that interannual variations are relatively weak in the EPFP but that seasonal variations are the strongest in the tropical Pacific, with a north/south seesaw pattern in the far EPFP (Figure 1). This seasonal cycle is almost entirely explained in the far EPFP by the first annual harmonic, which is still dominant in most of the EPFP except for a narrow band around 5°N where the semiannual signal overcomes it [*Boyer and Levitus*, 2002]. Large-scale analysis suggests that the SSS seasonal balance is mostly driven by precipitation in the part of the EPFP covered by the ITCZ, but more complex in the far east as advection and entrainment become important processes [*Bingham et al.*, 2010]. However, the few existing studies of

the eastern Pacific describing seasonal variations of SSS do not investigate their cause beyond rainfall [*Donguy and Hénin*, 1980; *Fiedler and Talley*, 2006]. Also, a couple of cruises give snapshots of strong SSS fronts at the southern and northern edge of the far EPFP [*Wooster*, 1969; *Tsuchiya and Talley*, 1998] but their presence has not been fully explored. SSS fronts and fresh pools are often associated in the tropics with strong salinity stratification which can impact SST, enhance ocean-atmosphere interactions and affect ENSO dynamics/thermodynamics through the barrier layer process, as in the western Pacific [*Lukas and Lindstrom*, 1991; *Vialard and Delecluse*, 1998; *Maes*, 1998; *Maes et al.*, 2002, 2005]. Global climatologies indeed confirm the seasonal occurrence of thick barrier layers in the far eastern Pacific [*de Boyer Montégut et al.*, 2007], suggesting a possible active role of salinity on regional ocean-atmosphere interactions.

[5] The strong spatial and seasonal variability of SSS in the eastern Pacific suggests a potentially important role of salinity on the regional climate. Moreover this large SSS variability provides a good test ground for the new Soil Moisture Ocean Salinity (SMOS) and Aquarius satellite
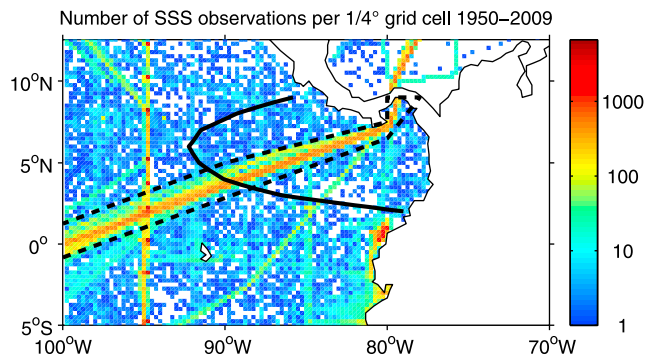
Figure 2. Density of SSS data, in number of observations per 1/4° bins (logarithmic scale). The data selection along the VOS track used for this study is delimited by the dashed lines. The black line indicates the mean position of the isohaline SSS = 33, i.e., the western boundary of the far EPFP.

missions dedicated to remote sensing of SSS. However, very little is known of the SSS dynamics in the eastern Pacific. As a first step, the main objectives of this paper are to investigate the seasonal dynamics of the far EPFP (later simply referred to as "fresh pool") and associated SSS fronts. Our approach is to describe the observed SSS variations, to summarize the main seasonal features of other relatively well known climatic variables and to identify their contribution to SSS variations.

2. Data Sets

[6] In situ near surface salinity (0–10 m) data used in this study, collected between 1950 and 2009, are from different sources depending on the time period. Over the 1950–2003 period, our collection includes bucket samples from Voluntary Observing Ships (VOS) [*Donguy and Hénin*, 1980], sporadic Nansen bottles, Salinity Temperature Depth (STD) and Conductivity Temperature Depth (CTD) from oceanographic cruises, and TAO/TRITON moorings [*Hayes et al.*, 1991]. Over the 1992–2003 period it includes, in addition, underway TSG (thermosalinograph) data from VOS [*Hénin and Grelet*, 1996]. Over the 2003–2009 period, VOS TSG benefit from an improved quality control (G. Alory et al., manuscript in preparation, 2012) and upper layer observations from the profiles collected by the Argo floats complete the set [*Roemmich and Owens*, 2000]. More details about these data, their processing and combination are given by *Delcroix et al.* [2005].

[7] This data set has been recently used to build a gridded SSS product for the tropical Pacific by optimal analysis [*Delcroix et al.*, 2011]. Although this product is useful for large-scale studies and reveals strong SSS variations in the far eastern Pacific (Figure 1), its spatial resolution (1° longitude, 1° latitude) and decorrelation scales (1600 km in longitude, 275 km in latitude) are too large to resolve the mesoscale features and fronts associated with the fresh pool. Figure 2 shows that the observation density is relatively inhomogeneous and low, except along a few ship tracks including several VOS tracks heading southwest from the Panama Canal mainly managed by the French SSS observation service, and a meridional track along 95°W used for maintenance of the TAO/TRITON moorings since 1992.

The best sampled VOS track is a direct line from Panama to 0°, 100°W (and further Tahiti) crossing the core of the EPFP. This high density VOS section (delimited by the dashed lines shown in Figure 2) is therefore selected to study the fresh pool. Underway VOS TSG data are 5-min medians with ship speeds of 15–20 knots which gives a resolution along track of about 2–3 km. Such a resolution makes individual ship crossings particularly suitable to capture the steep SSS fronts. We chose after several tests to divide the along track box in 0.25° bins in latitude and average all available SSS data for each calendar month in each bin (220 ± 125 observations per grid point). The final gridded latitude-month along track seasonal climatology of the fresh pool, which appears neither too noisy nor too smooth, is obtained by applying a 1/4–1/2–1/4 filter in latitude.

[8] Recently available SMOS remotely sensed SSS data are also used to evaluate their realism and their ability to provide SSS maps with homogeneous coverage, in space and time. The SMOS satellite mission supported by the European Space Agency (ESA) was launched in November 2009 [*Kerr et al.*, 2001]. The first gridded SSS research products, covering the whole 2010 year, were made available to the scientific community in September 2011. These products offer different spatial resolution from the 1/4° to 1°, and different temporal timescales from daily to monthly. Hereafter, we use the monthly composite data at the quarter of degree resolution obtained from the Ocean Salinity Expertise Center (CECOS) of the CNES-IFREMER Centre Aval de Traitement des Donnees SMOS (CATDS), at IFREMER, Plouzané, France [*Reul and Tenerelli*, 2011]. Note that SMOS satellite data are considered free of any land-induced contamination at distances larger than 150 km from the coastlines. The satellite is still in its calibration/validation phase and has to be checked against the ground truth. Our region of study, with strong spatial and temporal SSS variations relatively close to the coast, is a good testing ground. A regression on collocated VOS TSG and SMOS SSS data in this region over year 2010 is shown in Figure 3. The agreement between in situ and satellite data is relatively good: the
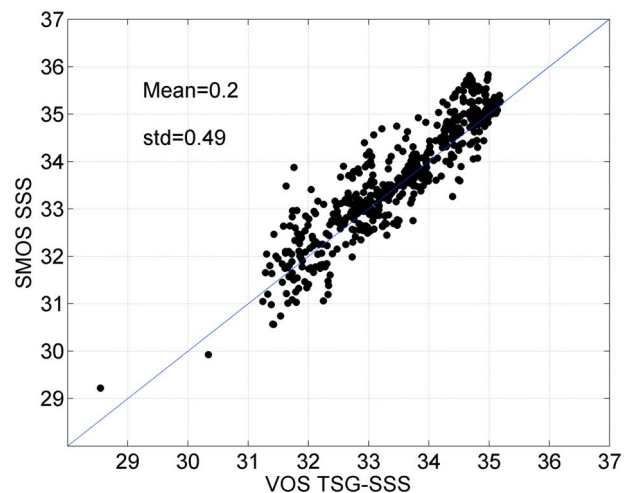
Figure 3. Regression between VOS TSG and SMOS SSS data in the region of study (Pacific region in Figure 2) for year 2010. Values of the mean and standard deviation of SMOS SSS difference with in situ SSS are reported.

0.2 positive bias of SMOS SSS (mostly found when SSS > 34) and 0.49 standard deviation of the differences between SMOS and TSG data are relatively weak compared to the range of SSS variations here (see below).

[9] SST is generally measured with SSS in situ. For consistency, SST data from the same in situ sources as SSS are therefore selected in the along track box. In the case of TSG measurements which include both SSS and SST, SST is corrected by substracting 0.2°C which is the estimated mean warm bias due to heating in the TSG circuit [*Delcroix and McPhaden*, 2002]. SST is processed the same way as SSS to produce a gridded latitude-month along track seasonal climatology. In addition, gridded climatological mean SST data at 1° resolution in longitude and latitude are extracted from the *World Ocean Atlas 2009* [*Locarnini et al.*, 2010] to set the large-scale context.

[10] Subsurface salinity and temperature data are issued from hydrographic profiles collected, validated and vertically interpolated to standard levels (every 5 m from 0 to 200 m) by the CORIOLIS operational oceanography center. They are distributed as part of the 2011 release of their global data set CORA-03 [*Gaillard et al.*, 2009]. Over the 2000–2010 period, Argo profiles represent the major subsurface data source, with additional data from CTD and moorings, which provides a relatively homogeneous spatial coverage. About 75% of these Argo profiles have been processed through a delayed mode quality control following the *Owens and Wong* [2009] method. In the Panama Bight, defined as the region of the Pacific east of 81°W between 2°S and 9°N [*Rodriguez-Rubio et al.*, 2003], more than 250 Argo profiles are available but only cover the 2003–2010 period. For each profile, the isothermal depth and mixed layer depth are estimated following *de Boyer Montégut et al.* [2007]. Namely, the isothermal depth is defined as the depth where the temperature is 0.2°C lower than the temperature at the reference depth of 10 m. The mixed layer depth is defined as the depth where, when compared to its value at 10 m, the potential density has increased by a threshold equivalent to the density difference due to a 0.2°C temperature change at constant salinity. Monthly seasonal climatology over the 2003–2010 period has been processed by averaging available data for each calendar month.

[11] Precipitation data are provided by the Tropical Rainfall Measuring Mission (TRMM). We use the 3B43 gridded product that combine both satellite and gauge data at the 0.25° by 0.25° resolution on monthly timescale over the 1998–2010 period [*Adler et al.*, 2000]. The monthly climatology has been processed by averaging available data for each calendar month during this period.

[12] High resolution (0.5°) Quikscat satellite wind and wind stress at the sea surface [*Ebuchi et al.*, 2002] are used to set the regional climatic context and to compute the wind-induced Ekman pumping.. Ekman pumping velocity (in m/day) is estimated using the same equation as *Kessler* [2002]: $W_{EK} = (curl(\tau)/f + \beta\tau^x/f^2)/\rho$, where τ is the surface wind stress and τ^x its East-West component, f is the coriolis parameter, $\beta = 2.2753 \times 10^{-11}$ (m s)$^{-1}$ and $\rho = 1025$ kg m^{-3}. Ekman pumping is not computed in the 3°N–3°S equatorial band due to the small value of the Coriolis parameter. Seasonal climatologies are computed for the 1999–2009 period.

[13] Two complementary data sets are used to describe the oceanic surface circulation in our region of study. The monthly gridded (1/3°) AVISO Ssalto/Duacs Sea Level Anomaly (SLA) [*Ducet et al.*, 2000] climatology, combining altimetric data from several satellite missions (Envisat, ERS1/2, TOPEX/Poseidon, Jason1–2), integrates seasonal variations in vertical stratification and surface geostrophic currents. A more direct view of the surface currents is obtained from the monthly gridded (1°) climatology of *Lumpkin and Garraffo* [2005], based on satellite-tracked drifters drogued at 15 m depth whose trajectories show the ability to capture coastal currents in the Panama Bight [*Chaigneau et al.*, 2006]. An along track climatology for these fields is produced by interpolation of the gridded products onto the mean ship track.

3. Data Analysis and Results

[14] Along track SSS and SST data from a few ship crossings along the Panama-Tahiti line for two well-sampled and contrasted months are shown in Figure 4 to give high-resolution snapshots of the surface conditions. In April, the fresh pool can be seen as a region with SSS around 32, separated from saltier waters by relatively well-marked SSS fronts on both its western and eastern side, respectively located around 90–95°W and 80–85°W. SST is around 29°C in the fresh pool at that time and shows an abrupt cooling (roughly 5°C) in the far east while a smoother SST front around 95–100°W marks the northern edge of the equatorial cold tongue. Both the western and eastern SSS and SST fronts roughly match each other. In December, the only SSS front is found at the western side of a coastal fresh pool where SSS is around 28–30, and is no more associated with a SST front. The near-equatorial SST front (95–100°W) is qualitatively similar as it was in April. West of 82.5°W, SST is cooler in December as compared to April. This cooling, reaching a maximum at the equator (i.e., 100°W), is consistent with the seasonal cycle of the cold tongue [*Mitchell and Wallace*, 1992]. The very different pictures for SSS and SST seasonal variations and associated fronts suggest that different processes are at work. The SSS front in December is at its strongest amplitude of the year, with a gradient sometimes larger than 4 over 1°, a step that is much larger than the one observed at the eastern edge of the western Pacific warm pool [*Picaut et al.*, 1996; *Eldin et al.*, 2004; *Maes*, 2008; *Bosc et al.*, 2009]. Comparing the April and December sections gives the annual range of displacement of the western front: up to 10° in longitude, or roughly 1200 km along track, which is also larger than observed for the western Pacific SSS front along the equator during non-ENSO years [*Delcroix and Picaut*, 1998]. Also, while seasonal variations obviously dominate the surface signals in the EPFP, note that SSS and SST sections show variations from year to year or within the same month (such as in April 2001). Therefore, interannual and intraseasonal variations also exist, but in situ data gaps make it difficult to distinguish these scales.

[15] The monthly mean seasonal cycle of SSS and SST are shown in Figure 5 along the southwest-northeast oriented VOS track. The seasonal cycle of SSS shows a strong freshening during the second half of the year east of 85°W resulting in a coastal fresh pool, then a southwestward displacement and erosion of this fresh pool during the first half of the following year in qualitative agreement with the low-resolution bucket SSS data analysis of *Donguy and Hénin*
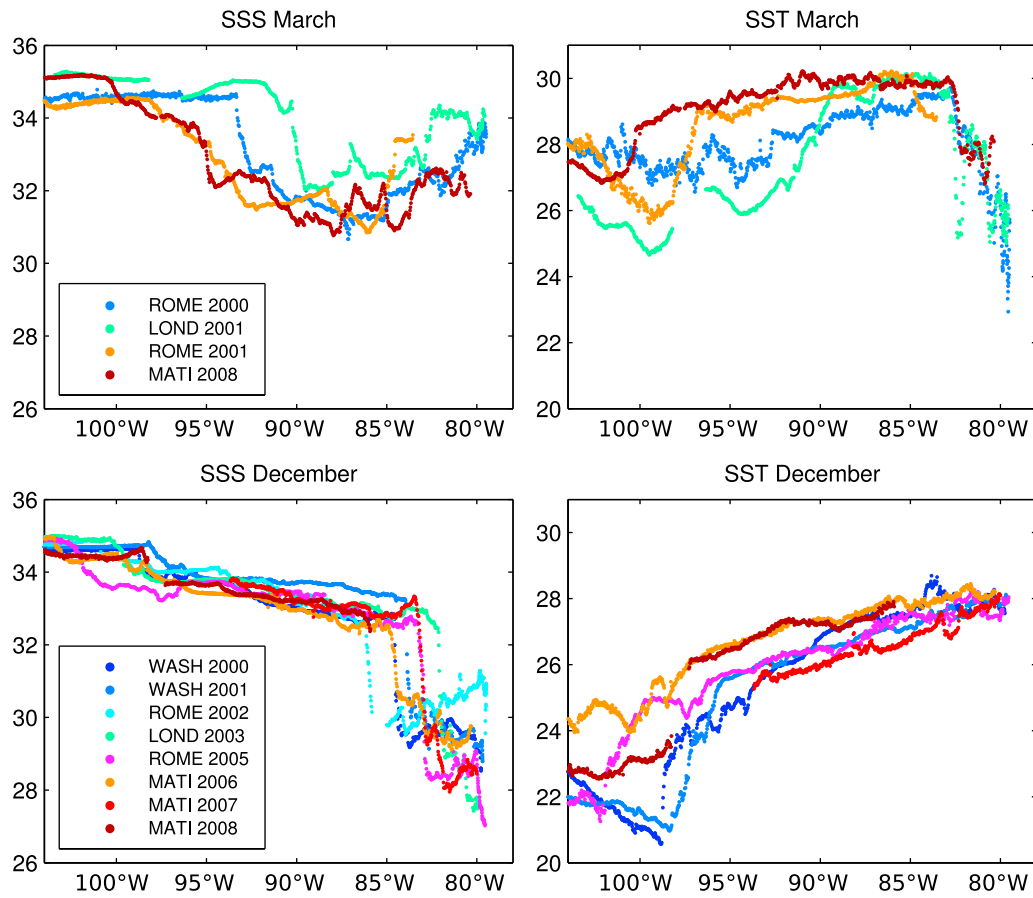
Figure 4. High-resolution SSS and SST transects collected from different Voluntary Observing Ships. The ship code and year of collect are given in the legends within the SSS figures.
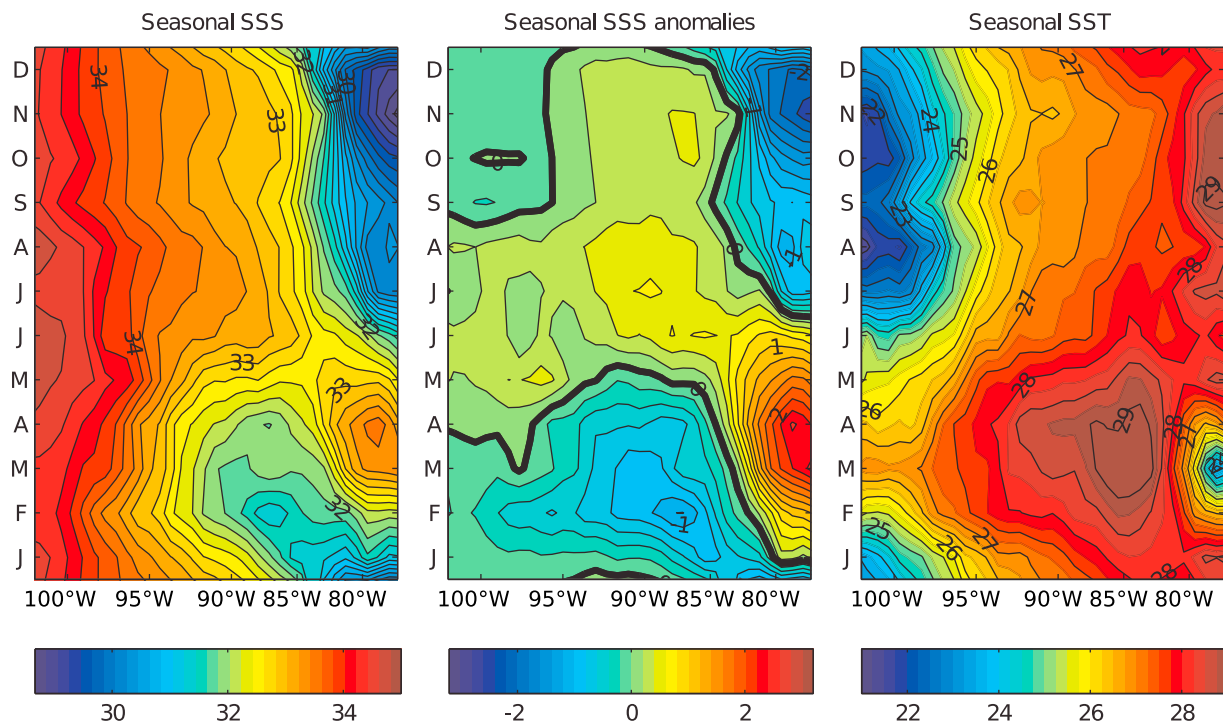
Figure 5. Seasonal climatology of along-track (left) SSS, (middle) SSS anomalies and (right) SST (°C).
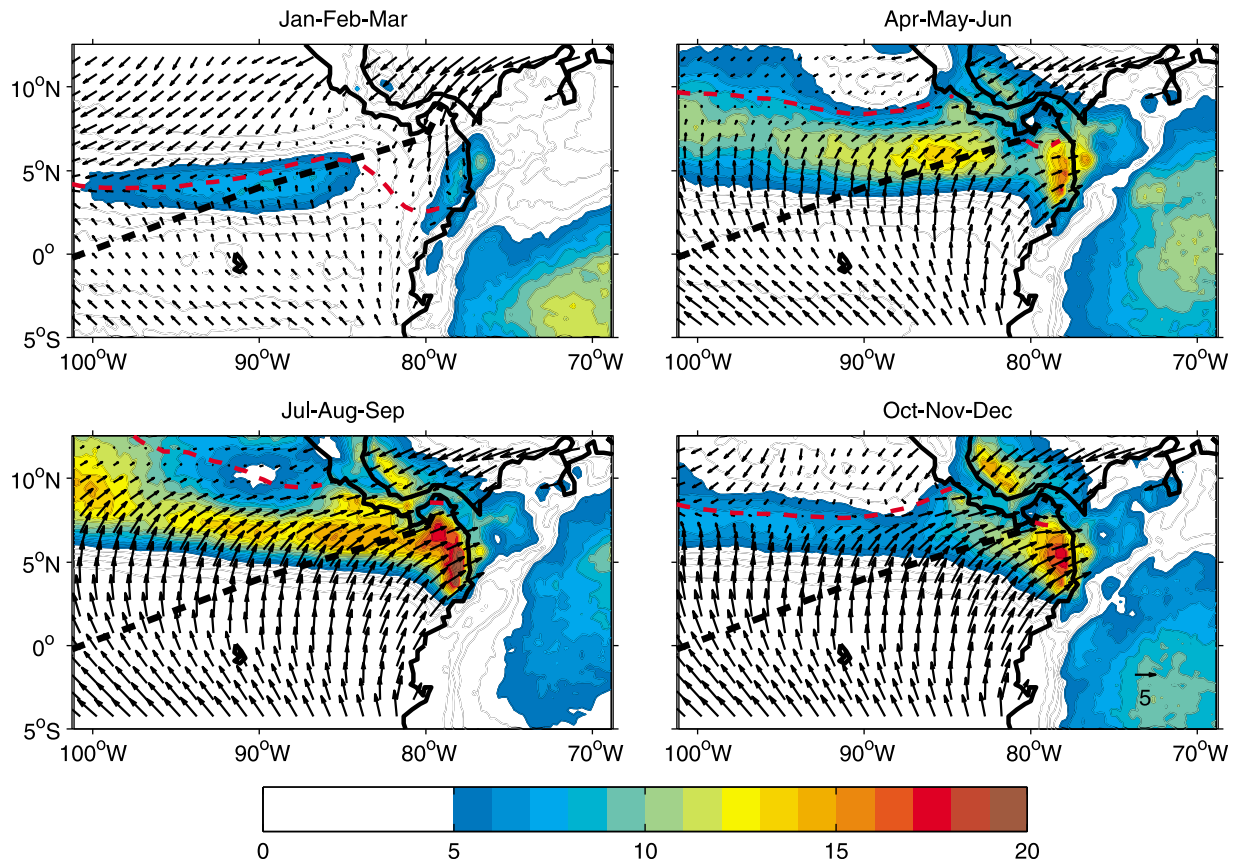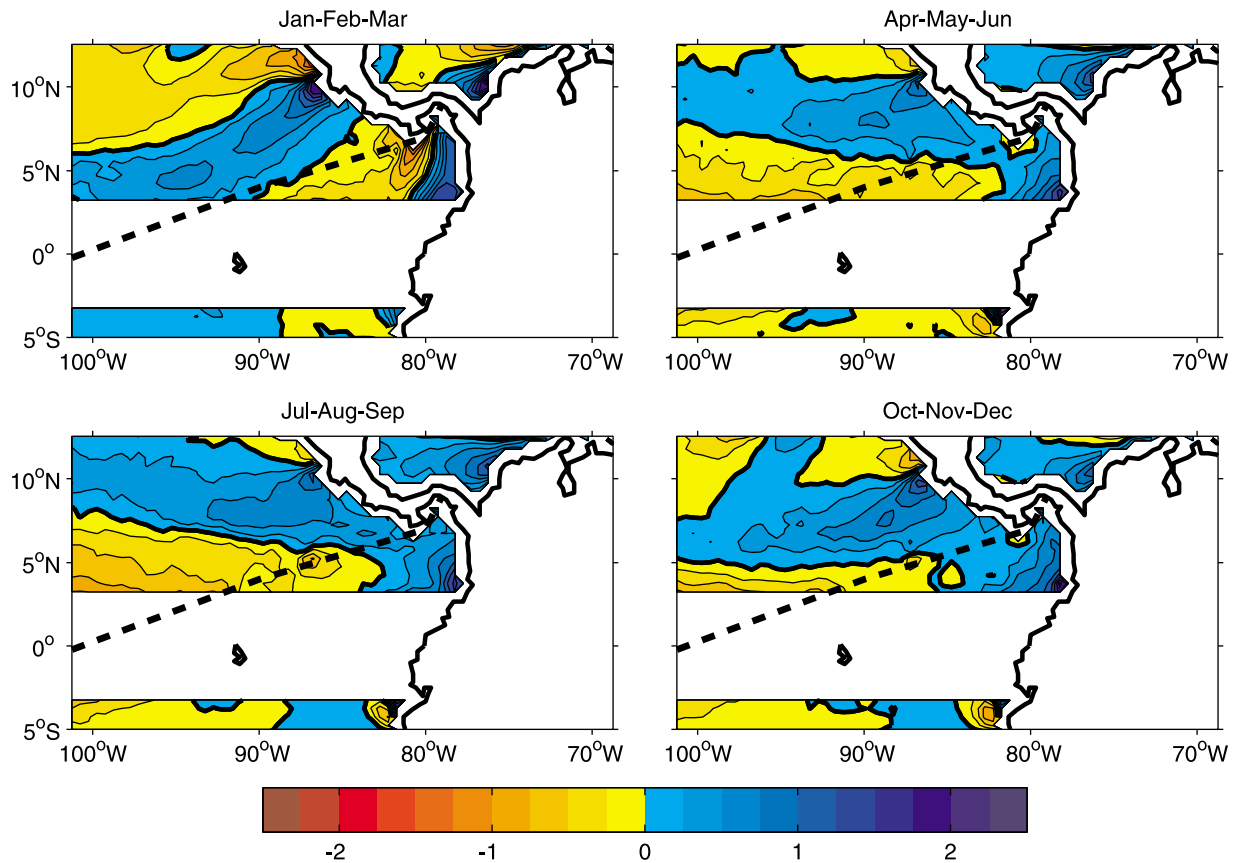
Figure 6. Seasonal climatology of Quikscat surface wind (m/s, arrows) and TRMM rain (mm/d, colors), with VOS track (dashed black line) and ITCZ (defined at each longitude as the latitude where meridional winds converge, dashed red line) overlaid.

[1980, Figure 11]. This is also consistent with the mooring data at 3.5°N, 95°W (slightly north of the VOS line) showing a surface freshening down to 33 or even less between February and May [*McPhaden et al.*, 2008, Figure 2]. The largest seasonal amplitude and lowest SSS values (<30 from October to December) are found just off the Panama Canal, in good agreement with coastal measurements [*Linsley et al.*, 1994, Figure 4]. The strongest SSS front is found around the 32 isohaline. While no SST front is associated with this SSS front, high SST (>28°C) is generally associated with SSS lower than 32. There is an abrupt increase in salinity and cooling in the far East in winter which produces the March/April seasonal maximum SSS and minimum SST found here: SSS > 33 and SST < 24°C respectively. Note that the SST minimum precedes the SSS maximum by one month. This seasonal cooling was already shown by *Legeckis* [1986] using in situ observations. The fresh pool almost disappears along this track in May before it starts reappearing in June in the far east. West of 95°W (i.e., south of 2°N), the seasonal cycle is particularly strong for SST, while relatively weak for SSS. This corresponds to variations of equatorial upwelling in the cold tongue region [e.g., *Mitchell and Wallace*, 1992; *Wang*, 1994; *Fu and Wang*, 2001]. At the northern edge of this cold tongue, a strong SST front can be seen around the 24°C isotherm [*de Szoeke et al.*, 2007]. While weaker and less variable than further east, a secondary SSS front is found around the 34 isohaline, a point that was also noticed by early studies [*Wooster*, 1969; *Donguy and Hénin*, 1980].

[16] To correlate with the atmospheric regional conditions, the climatological mean surface wind and rain are shown for the four seasons in Figure 6. Over the eastern Pacific Ocean, the wind and rain patterns are dominated by the presence of the almost zonally oriented ITCZ, where southeastern and northeastern trade winds converge and atmospheric convection occurs, generating a nearby meridional maximum in rainfall. The precipitation maximum is located south of the ITCZ as atmospheric convection depends both on wind convergence and SST [e.g., *Xie et al.*, 2005]. Near the coast, strong ocean-atmosphere-land interactions, including local topographic effects and large-scale differential heating between the ocean and North American landmass, result in a more complex picture [*Amador et al.*, 2006]. Over the isthmus of Central America, the seasonal variations are typical of a monsoon regime [*Hsu et al.*, 2011].

[17] The strongest rains are found from spring to fall, with a summer peak of 20 mm/day in the Panama Bight. They are associated with the northern-most position of the ITCZ which brings strong and moisture-laden Pacific winds toward the Panama-Colombia coast and mountain ranges, most notably the eastward Chocó jet around 5°N which is responsible for some of the world's largest annual rainfall records in coastal Colombia [*Poveda and Mesa*, 2000]. Note that the local summer rain minimum around 10°N, 90°W is due to reduced convection over the cold SST patch associated with the Costa Rica thermocline dome [*Xie et al.*, 2005]. It is obvious from the location of these rains and

Figure 7. Seasonal climatology of Ekman pumping (m/d) computed from Quikscat surface winds, with VOS track (dashed line) overlaid.

their seasonality that they are responsible for the formation of the fresh pool.

[18] However, the cumulative contribution of river inputs is not negligible in the Panama Bight. The total runoff was estimated as 350 km^3/yr [*Forsbergh*, 1969] while TRMM precipitation amounts to 825 km^3/yr when integrated over the Panama Bight. Rivers therefore contribute to 30% of the total freshwater input. Due to the proximity of the Cordillera to the coast, rivers are numerous but short, with the largest one located at 4°N. Their main effect is to bring coastal rains to the ocean along the mountain slope with no significant lag, which generates strong SSS gradients running parallel to the Colombian coast [*Forsbergh*, 1969]. It also probably contributes to the summer-fall freshening at the eastern end of the VOS line.

[19] In contrast, the southern-most (5°N) position of the ITCZ in winter corresponds to a dry season in the eastern tropical Pacific, due to orographic subsidence when the northeasterly trade winds impinge on Central American mountains [*Xu et al.*, 2005]. These winds are also intensified when channeled through gaps in the Central American Cordillera, creating strong jets like the Papagayo gap wind around 10°N, and the Panama gap wind around 8°N at the northern entrance of the Bight [*Chelton et al.*, 2000a, 2000b]. These strong winds can locally enhance evaporation, oceanic mixing and affect currents through wind curl induced Ekman pumping [*Sun and Yu*, 2006; *Liang et al.*, 2009]. Of particular importance, the Panama gap wind,

which peaks in January and lasts until April, generates a cold SST patch in its wake (Figure 5) that inhibits convection and breaks the winter ITCZ into two parts (Figure 6). These latter points are also discussed in details by *Xie et al.* [2005].

[20] To investigate the wind effect on oceanic currents and vertical stratification, the seasonal climatology of Ekman pumping was computed from high-resolution wind stress (Figure 7). A zonal band of upward (positive) Ekman pumping is found all-yearlong under the ITCZ and follows its seasonal migration. Upward pumping is also found along the Colombian coast, while downward pumping is found elsewhere. North of 5°N, the positive and negative maximum in Ekman pumping are found in winter near the Central American coast at the exit of mountain gaps: strong gap winds generate curl and therefore Ekman pumping dipoles [*Kessler*, 2006], with upward pumping on their left flank and downward pumping on their right flank (when looking downwind). The Ekman pumping dipole associated with the Papagayo gap wind, although stronger in winter, can in fact be seen all year-round, while the signature of the Panama gap wind is only clear in winter.

[21] Sea Level Anomalies (SLA) are directly related to changes in thermocline depth in a 2-layer tropical upper ocean, and can reflect both local wind-forcing and remote forcing transmitted through planetary waves. The seasonal climatology of SLA is presented in Figure 8. In the second half of the year, far from the coast (west of 90°W) and off the equator (north of 2°N), positive SLA roughly follows
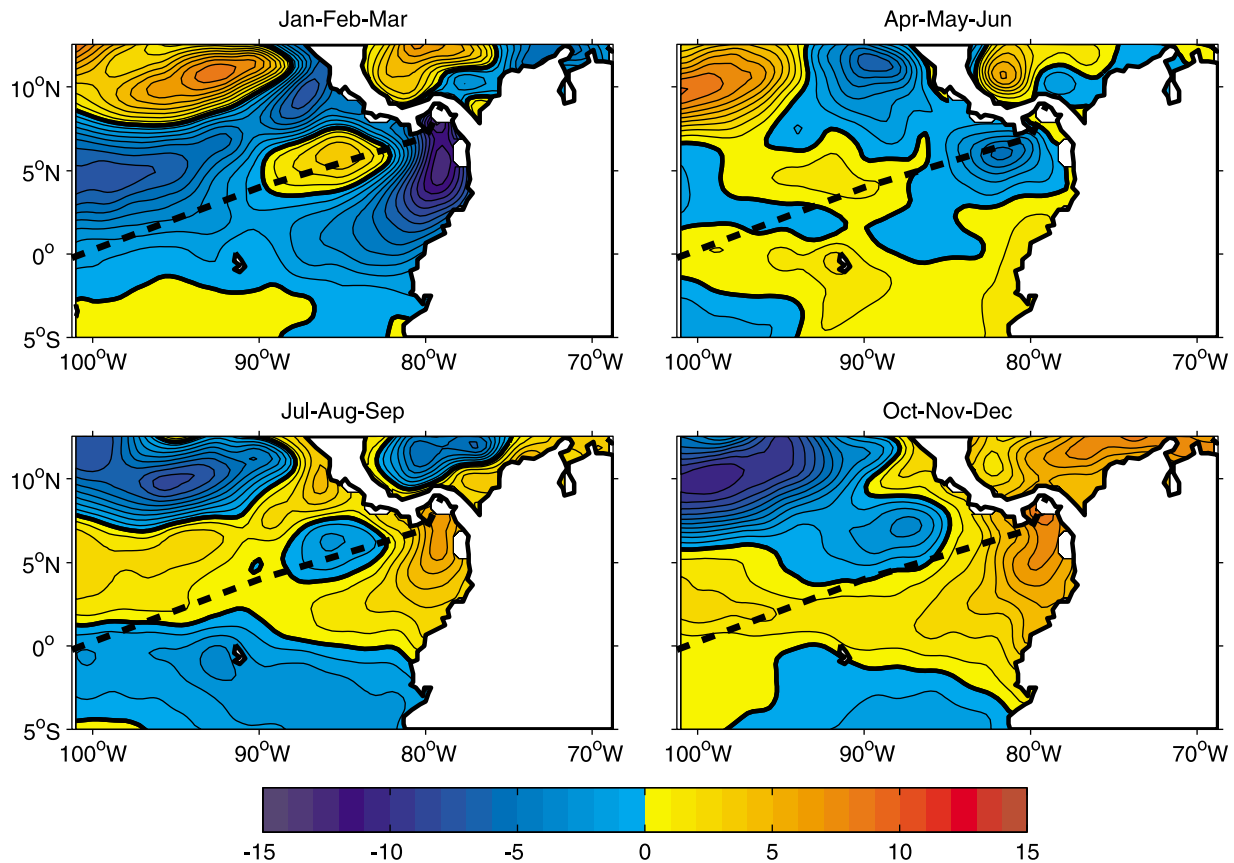
**Figure 8.** Seasonal climatology of AVISO sea level anomalies (cm), with VOS track (dashed line) overlaid.

downward Ekman pumping patterns and conversely, as expected from local wind-forcing. In winter, SLA dipoles clearly reflect the Ekman pumping dipoles generated by the Papagayo and Panama gap winds. Although contrary to pumping dipoles, SLAs are not trapped to the coast but peak further offshore in the form of eddies. This is probably due to the slow southwestern propagation of sea level and thermocline anomalies, under the combined effect of wind-forcing and Rossby waves [*Kessler*, 2006]. The negative SLA eddy located around 10°N all yearlong corresponds to the Costa Rica thermocline dome, which has a strong impact on the local climate and biology, and is generated by the Papagayo gap wind [*Hofmann et al.*, 1981; *Fiedler*, 2002; *Xie et al.*, 2005].

[22] As strong SSS and SLA variations (Figures 5 and 8) both occur at seasonal timescales around 80°W, this result suggests a link between surface and subsurface salinity variations. To clarify this link, the seasonal cycle of subsurface salinity computed from hydrographic profiles is shown in this region (Figure 9). Salinity increases with depth until it reaches nearly constant values of 35 below 60 m. At the surface, the summer decrease and winter increase in the salinity observed at the eastern end of the VOS track are also clearly seen in subsurface data. While the density mixed layer depth is roughly constant (10–15 m) all yearlong, the thermocline (as represented by the 20°C isotherm) which is around 50 m deep in summer-fall abruptly rises in winter to reach the mixed layer in March. The seasonal cycle of the thermocline depth is consistent with SLA data in the Panama Bight (Figure 8). The 34.5 isohaline follows the vertical displacement of the thermocline, which indicates upward advection of a water mass in winter. This upwelling is associated with negative SLA (Figure 8) and obviously driven by the winter Panama gap wind (Figure 6) through Ekman pumping (Figure 7) in the Panama Bight [*Forsbergh*, 1969; *Legeckis*, 1988; *Devis-Morales et al.*, 2008]. The 2-month lag between the gap wind and upwelling peak suggests an oceanic adjustment to the wind stress. The winter upwelling is probably responsible for the erosion of the fresh pool at its eastern boundary, SSS maximum and SST minimum east of 82.5°W along the VOS line (Figure 5). While upwelling of cool and salty waters peaks in March, in phase with the SST minimum, the 1-month lag of the SSS maximum could be due to enhanced evaporation under the gap wind.

[23] Also, while the density mixed layer depth matches the isothermal layer depth in March, they are quite different during fall and separated by a barrier layer due to the strong haline stratification under the fresh pool at that time of year. The presence of barrier layer in this region is consistent with the available global gridded climatology [*de Boyer Montégut et al.*, 2007] and can have important effects on the surface dynamics and thermodynamics of the surface layer by insulating it from the deeper and colder waters, as it has been shown in the western Pacific warm pool [*Lukas and Lindstrom*, 1991; *Vialard and Delecluse*, 1998; *Maes et al.*, 2002; *Bosc et al.*, 2009].

Salinity in Panama Bight
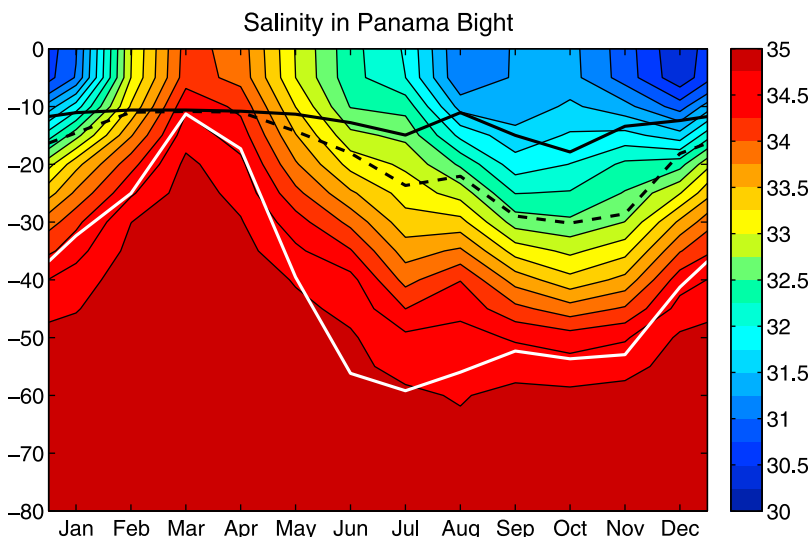
Figure 9. Seasonal cycle of subsurface salinity (colors), mixed layer depth (thick black line), isothermal layer depth (dashed black line) and 20°C isotherm depth (white line) from hydrographic profiles collected in the Panama Bight (east of 81°W between 2°S and 9°N).

[24] Surface currents (Figure 10) can also affect seasonal SSS variations by advecting salinity gradients, particularly strong at the boundary of the fresh pool. The region of study is located at the eastern boundary of the equatorial Pacific current system. The surface circulation is dominated by well known large-scale currents west of 90°W: the westward SEC south of 5°N with two branches separated by a minimum slightly south of the equator, the eastward North Equatorial Counter-Current (NECC) between 5°N and 8°N, the westward North Equatorial Current (NEC) around 10°N. While
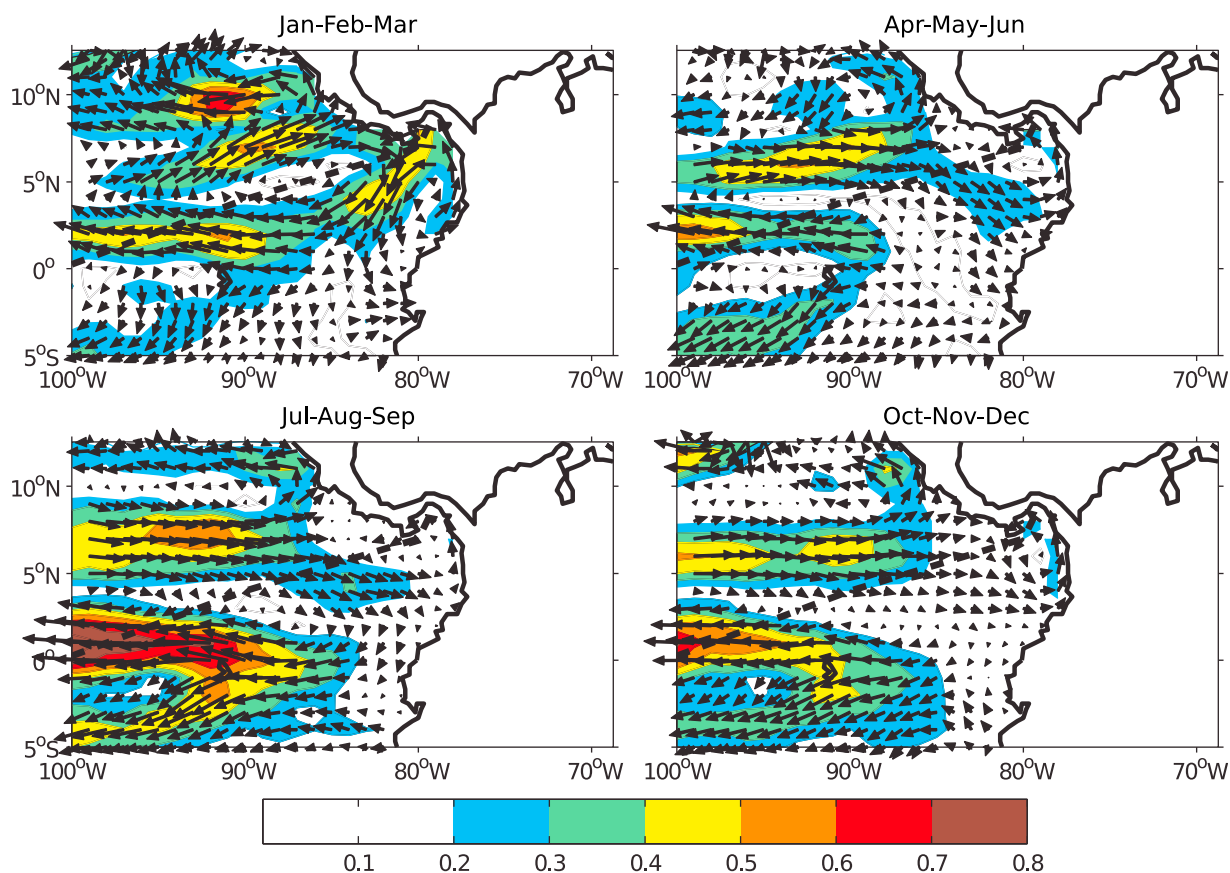
Figure 10. Seasonal climatology of surface currents from Lagrangian drifters (arrows, current vectors; colors, amplitude in m/s), with VOS track (dashed line) overlaid.
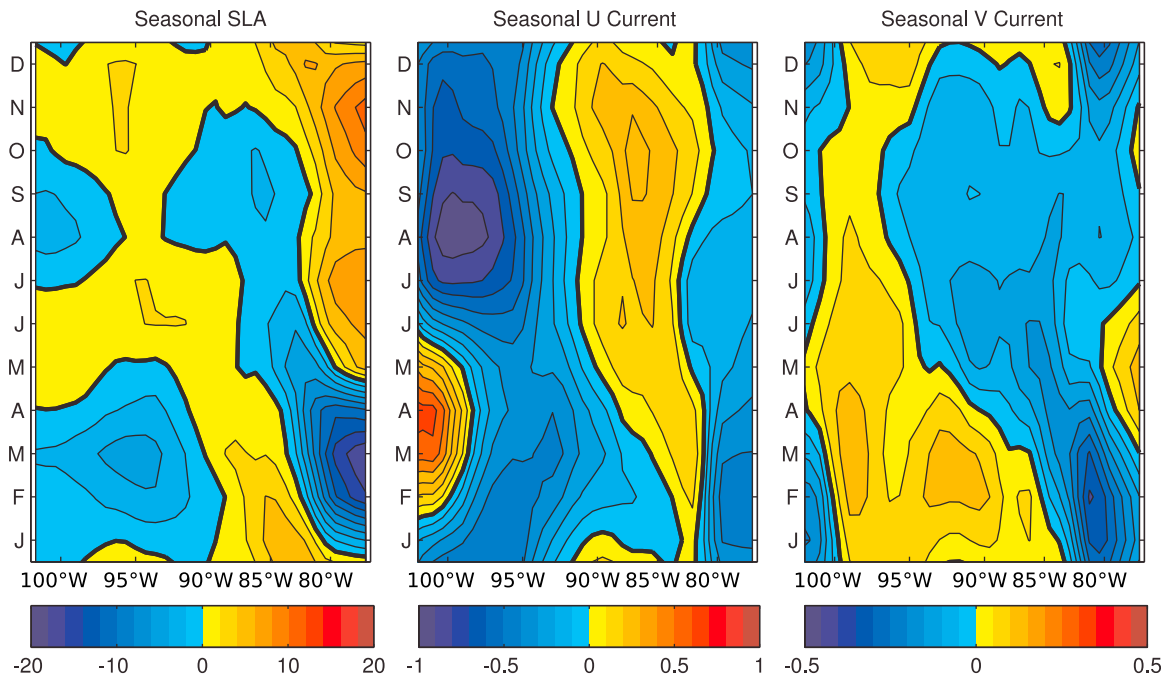
Figure 11. Seasonal climatology of (left) sea level anomalies (cm), (middle) zonal and (right) meridional surface currents (m/s) from drifters along the VOS track. Note that the color bars differ between the zonal and meridional currents.

in the open ocean, the NECC and the ITCZ are closely associated zonal structures, the picture is complicated here by the presence of land and gap winds. The eastern termination of the equatorial current system and connection between currents is complex and not well known [*Kessler*, 2006]. The coastal currents are relatively weak. The northwestward Costa Rica Coastal Current (CRCC) can be seen connecting the NECC to the NEC. The Panama Bight Cyclonic Gyre (PBCG) [*Chaigneau et al.*, 2006] is present most of the year, although high-resolution regional studies show that the geostrophic circulation can reverse to cyclonic during summer here [*Rodriguez-Rubio et al.*, 2003; *Devis-Morales et al.*, 2008]. The PBCG can advect low-salinity waters from the Colombian coast, where rainfall and river runoff reach a regional maximum, to the north of the Panama Bight. This could reinforce coastal freshening at the eastern end of the VOS line during the rainy season, in addition to local rainfall and runoff.

[25] In winter, the gap winds have a strong effect on coastal circulation (Figure 10). As already suggested by SLA (Figure 8), they generate a dipole of eddies with clockwise (anticyclonic) circulation on their right flank, anticlockwise (cyclonic) circulation on their left flank, and a strong current under the wind peak and in the same direction. In this way, the Panama gap wind reinforces the PBCG. It also connects the eastern end of the NECC to the SEC through an eastward coastal current and southwestward current found directly under the wind jet. The Papagayo gap wind connects the NECC to a strongly intensified NEC through the CRCC. This cyclonic circulation is associated with the Costa Rica Dome (Figure 8) through geostrophy. The NECC changes its path from eastward to northeastward in winter under the effect of these two gap winds and feeds both eddy systems. The rest of the year, the circulation is mostly zonal, the

coastal currents weaker and the connection between the SEC and NECC is less obvious.

[26] The winter intensification of the currents near the coast by the gap winds suggests an important role of horizontal advection on the coastal fresh pool which developed during the summer-fall rainy season. The strong winter PBCG is associated with upward Ekman pumping (Figure 7) and therefore upwelling in the Panama Bight which quickly increases SSS in this region after the rainy season and consequently erodes the eastern side of the fresh pool (Figures 5 and 9). The strong southwestward jet generated under the Panama gap wind at the same time is likely to advect these positive SSS anomalies further offshore and particularly along the VOS line, as seen in Figure 5 during winter-spring. The enhanced evaporation associated with the strong winds may also contribute to the increase in salinity and cooling.

[27] To better evaluate the respective role of the 3 components of advection on the seasonal SSS variations, the SLA (which reflects vertical advection), the zonal and meridional components of the surface currents are projected along the VOS line (Figure 11) and compared to the along track SSS variations (Figure 5). The largest SLAs are found at the eastern boundary. They are maximum and negative in winter and reflect the upward Ekman pumping in the Panama Bight driven by the gap wind. They slowly propagate westward along the track until about 85°W, which is consistent with the southwestward propagation of thermocline anomalies in this region shown by *Kessler* [2006] and attributed to a combination of local wind stress curl forcing and Rossby waves. The upward advection associated with these SLAs can explain the winter increase in salinity in Panama Bight and subsequent eastern erosion of the fresh pool until it mostly disappears in June. The positive SLAs along the coast also
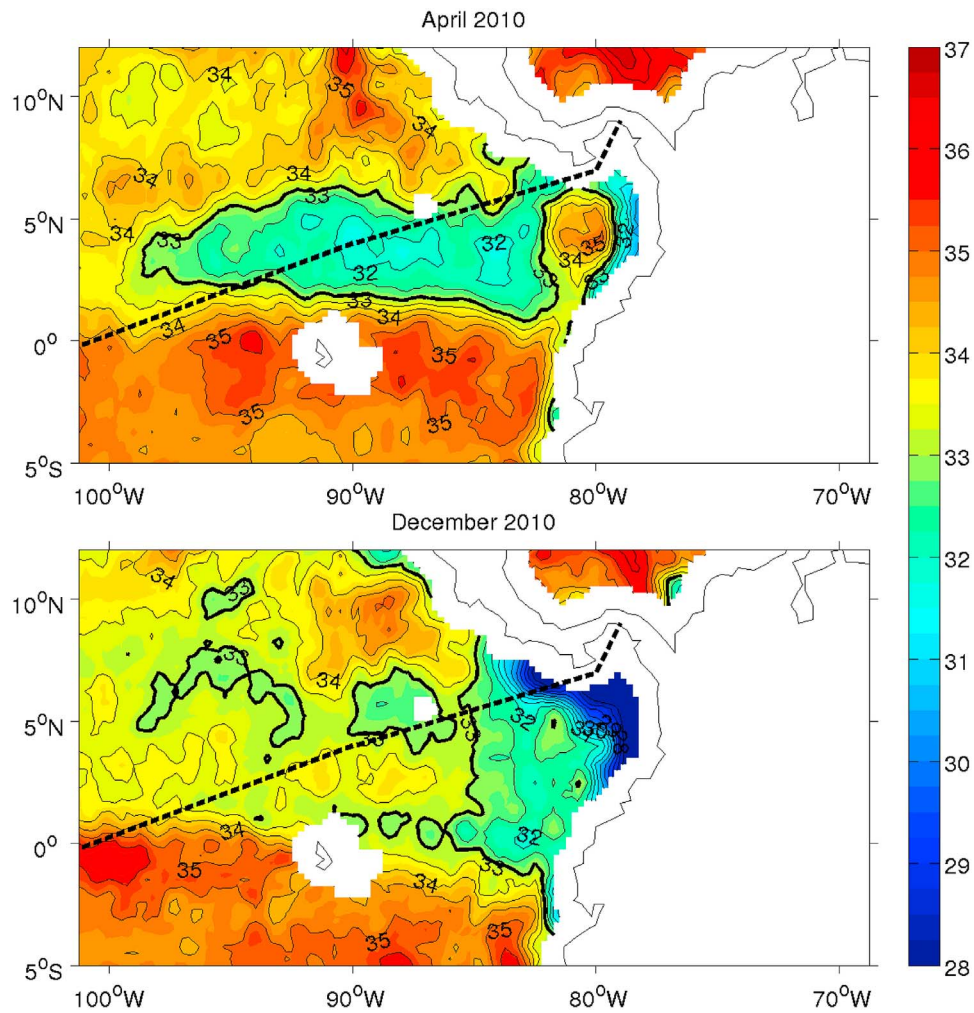
Figure 12. Monthly analyses of SSS as reconstructed from the SMOS remote sensing mission in (top) April and (bottom) December 2010, with VOS track (dashed line) superimposed.

propagate westward in fall-winter but the corresponding downwelling anomalies are not expected to affect SSS much.

[28] The relative part of zonal and meridional advection is not easy to quantify as zonal and meridional SSS gradients cannot be simply estimated from the available data. However, considering the large-scale zonal gradient which corresponds to a strong eastward decrease of SSS during the second half of the year, the NECC eastward velocity between 90°W and 80°W at that time (Figures 10 and 11) probably helps maintaining a sharp SSS front and a fresh pool trapped to the coast. In contrast, the NECC shifts north of the VOS line in winter and is largely replaced by a westward flow associated with the PBCG and the SEC, which probably contributes to the westward spreading of the fresh pool and associated front. While meridional component of the currents is generally smaller than the zonal current along the VOS track, the climatological mean salinity gradients at the boundaries of the fresh pool are larger in the meridional than in the zonal direction (Figure 1), therefore meridional advection must be considered too. The meridional velocity is maximum and southward in winter under the Panama gap wind near 80°W (Figure 11). This current, between the cyclonic and anticyclonic eddies generated by

the gap wind (Figure 10), probably also contributes to the observed winter increase in SSS by bringing saltier waters either upwelled in the PBCG or advected by the NECC. Even if it is not possible to quantify the relative contribution of zonal, meridional and vertical advection on seasonal SSS variations with available observations, it seems that all three components of current constructively combine to maintain, then to expand westward, and eventually to destroy the fresh pool during the seasonal cycle.

4. Conclusion

[29] The lowest salinity waters in the tropical Pacific are found off Panama in the far eastern Pacific fresh pool, where SSS is lower than 33 all yearlong. By focusing on seasonal SSS variations along a well-sampled VOS line, we showed that this fresh pool dynamically responds to strong regional ocean-atmosphere-land interactions. First, monsoon rains (and associated river runoff) give birth to the fresh pool in the Panama Bight during summer and fall. Second, strong currents driven by topography-induced winds expand it westward in winter and eventually destroy it from the east, by mixing with upwelled saltier waters. The same dynamics also generate steep SSS fronts at the edges of the fresh pool.

[30] The SSS fronts associated with the fresh pool and the amplitude of its seasonal cycle are large enough to suggest they could be detected by the new satellite missions for remote sensing of SSS. Compared to in situ data, SMOS satellite data provide a more homogeneous coverage which gives access to high-resolution SSS maps for the open ocean. The validation of SMOS data with collocated in situ observations in our region of study is really encouraging (Figure 3). SMOS SSS maps for April and December 2010 are presented in Figure 12. As seasonal variations are dominant in the region, it makes sense to compare these maps with the along track climatological seasonal cycle (Figure 5), although no direct comparison along the VOS line can be done east of 82°W due to the SMOS coastal mask. Remarkably, all the major features shown with in situ data are well reproduced in the present SMOS analysis: the westward expansion of the fresh pool (SSS < 33) from 85°W in December to 95°W in April, the steep SSS front east of the 32 isohaline and SSS minimum of 28 in the Panama Bight in December, the strong SSS increase to around 35 in the Panama Bight in April. Moreover, SSS changes occurring between December and April are qualitatively consistent with the expected effects of winter climatological currents (Figure 10), including the Panama Bight upwelling. SMOS maps also confirm that the VOS line is by chance well located to monitor the main seasonal features of the fresh pool. Interestingly, SMOS data are able to detect other mesoscale features in the region such as the near-equatorial SSS front or the local SSS maximum in the Costa Rica dome, which looks promising for future studies.

[31] The present study explores qualitatively the seasonal dynamics of the fresh pool. Quantifying the relative contribution of the different mechanisms on SSS variations would require a mixed layer salt budget. A model would be an appropriate tool for that. Also, the regional occurrence of SSS fronts and barrier layers suggests, by analogy with the western tropical Pacific, a link between surface and subsurface salinity which could give additional value to the satellite SSS data [*Maes*, 2008; *Bosc et al.*, 2009]. As barrier layers can play an active role on the tropical climate [e.g., *Maes et al.*, 2002, 2005], studying their impacts in the region seems worthwhile. This could be done through regional modeling combined with analysis of subsurface/surface in situ and satellite data. Also, interannual variations of the fresh pool, even if quantitatively smaller than its seasonal variations, need further investigation as ENSO is a strong climate driver in the eastern Pacific. At longer timescales, it is also important to monitor SSS in the eastern Pacific as it makes a good oceanic rain gauge of our changing water cycle [*Cravatte et al.*, 2009; *Yu*, 2011], and therefore to maintain a continuous observation network in the region.

References

Adler, R. F., G. J. Huffman, D. T. Bolvin, S. Curtis, and E. J. Nelkin (2000), Tropical rainfall distributions determined using TRMM combined with other satellite and rain gauge information, *J. Appl. Meteorol.*, *39*(12), 2007–2023, doi:10.1175/1520-0450(2001)040<2007:TRDDUT>2.0.CO;2.

Amador, J. A., E. J. Alfaro, O. G. Lizano, and V. O. Magaña (2006), Atmospheric forcing of the eastern tropical Pacific: A review, *Prog. Oceanogr.*, *69*(2–4), 101–142, doi:10.1016/j.pocean.2006.03.007.

Ballance, L. T., R. L. Pitman, and P. C. Fiedler (2006), Oceanographic influences on seabirds and cetaceans of the eastern tropical Pacific: A review, *Prog. Oceanogr.*, *69*(2–4), 360–390, doi:10.1016/j.pocean.2006.03.013.

Bennett, E. B. (1966), Monthly charts of surface salinity in the eastern tropical Pacific Ocean, *Bull. Inter-Am. Trop. Tuna Comm.*, *11*(1), 1–44.

Benway, H. M., and A. C. Mix (2004), Oxygen isotopes, upper-ocean salinity, and precipitation sources in the eastern tropical Pacific, *Earth Planet. Sci. Lett.*, *224*, 493–507, doi:10.1016/j.epsl.2004.05.014.

Bingham, F. M., G. R. Foltz, and M. J. McPhaden (2010), Seasonal cycles of surface layer salinity in the Pacific Ocean, *Ocean Sci.*, *6*, 775–787, doi:10.5194/os-6-775-2010.

Bosc, C., T. Delcroix, and C. Maes (2009), Barrier layer variability in the western Pacific warm pool from 2000 to 2007, *J. Geophys. Res.*, *114*, C06023, doi:10.1029/2008JC005187.

Boyer, T. P., and S. Levitus (2002), Harmonic analysis of climatological sea surface salinity, *J. Geophys. Res.*, *107*(C12), 8006, doi:10.1029/2001JC000829.

Chaigneau, A., R. Abarca del Rio, and F. Colas (2006), Lagrangian study of the Panama Bight and surrounding regions, *J. Geophys. Res.*, *111*, C09013, doi:10.1029/2006JC003530.

Chelton, D. B., M. H. Freilich, and S. K. Esbensen (2000a), Satellite observations of the wind jets off the Pacific coast of Central America. Part I: Case studies and statistical characteristics, *Mon. Weather Rev.*, *128*, 1993–2018, doi:10.1175/1520-0493(2000)128<1993:SOOTWJ>2.0.CO;2.

Chelton, D. B., M. H. Freilich, and S. K. Esbensen (2000b), Satellite observations of the wind jets off the Pacific coast of Central America. Part II: Regional relationships and dynamical considerations, *Mon. Weather Rev.*, *128*, 2019–2043, doi:10.1175/1520-0493(2000)128<2019:SOOTWJ>2.0. CO;2.

Cravatte, S., T. Delcroix, D. Zhang, M. McPhaden, and J. LeLoup (2009), Observed freshening and warming of the western Pacific warm pool, *Clim. Dyn.*, *33*, 565–589, doi:10.1007/s00382-009-0526-7.

de Boyer Montégut, C., J. Mignot, A. Lazar, and S. Cravatte (2007), Control of salinity on the mixed layer depth in the world ocean: 1. General description, *J. Geophys. Res.*, *112*, C06011, doi:10.1029/2006JC003953.

Delcroix, T., and M. McPhaden (2002), Interannual sea surface salinity and temperature changes in the western Pacific warm pool during 1992–2000, *J. Geophys. Res.*, *107*(C12), 8002, doi:10.1029/2001JC000862.

Delcroix, T., and J. Picaut (1998), Zonal displacement of the western equatorial Pacific fresh pool, *J. Geophys. Res.*, *103*, 1087–1098, doi:10.1029/97JC01912.

Delcroix, T., M. J. McPhaden, A. Dessier, and Y. Gouriou (2005), Time and space scales for sea surface salinity in the tropical oceans, *Deep Sea Res., Part I*, *52*(5), 787–813, doi:10.1016/j.dsr.2004.11.012.

Delcroix, T., G. Alory, S. Cravatte, T. Corrège, and M. J. McPhaden (2011), A gridded sea surface salinity data set for the tropical Pacific with sample applications (1950–2008), *Deep Sea Res., Part I*, *58*(1), 38–48, doi:10.1016/j.dsr.2010.11.002.

de Szoeke, S. P., S.-P. Xie, T. Miyama, K. J. Richards, and R. J. O. Small (2007), What maintains the SST front north of the eastern equatorial cold tongue?, *J. Clim.*, *20*, 2500–2514, doi:10.1175/JCLI4173.1.

Devis-Morales, A., W. Schneider, R. A. Montoya-Sánchez, and E. Rodríguez-Rubio (2008), Monsoon-like winds reverse oceanic circulation in the Panama Bight, *Geophys. Res. Lett.*, *35*, L20607, doi:10.1029/2008GL035172.

Donguy, J. R., and C. Hénin (1980), Surface conditions in the eastern equatorial Pacific related to the intertropical convergence zone of the winds, *Deep Sea Res., Part A*, *27*, 693–714, doi:10.1016/0198-0149(80)90023-0.

Ducet, N., P. Le Traon, and G. Reverdin (2000), Global high-resolution mapping of ocean circulation from TOPEX/Poseidon and ERS-1 and -2, *J. Geophys. Res.*, *105*(C8), 19,477–19,498, doi:10.1029/2000JC900063.

Ebuchi, N., H. C. Graber, and M. J. Caruso (2002), Evaluation of wind vectors observed by QuikScat/SeaWinds using ocean buoy data, *J. Atmos. Oceanic Technol.*, *19*(12), 2049–2062, doi:10.1175/1520-0426(2002)019<2049:EOWVOB>2.0.CO;2.

Eldin, G., T. Delcroix, and M. Rodier (2004), The frontal area at the eastern edge of the western equatorial Pacific warm pool in April 2001, *J. Geophys. Res.*, *109*, C07006, doi:10.1029/2003JC002088.

Fiedler, P. C. (2002), The annual cycle and biological effects of the Costa Rica Dome, *Deep Sea Res., Part I*, *49*, 321–338, doi:10.1016/S0967-0637(01)00057-7.

Fiedler, P. C., and L. D. Talley (2006), Hydrography of the eastern tropical Pacific: A review, *Prog. Oceanogr.*, *69*(2–4), 143–180, doi:10.1016/j.pocean.2006.03.008.

Forsbergh, E. D. (1969), On the climatology, oceanography, and fisheries of the Panama Bight, *Bull. Inter-Am. Trop. Tuna Comm.*, *14*, 49–385.

Fu, X., and B. Wang (2001), A coupled modeling study of the seasonal cycle of the Pacific cold tongue. Part I: Simulation and sensitivity experiments, *J. Clim.*, *14*, 765–779, doi:10.1175/1520-0442(2001)014<0765:ACMSOT>2.0.CO;2.

Gaillard, F., E. Autret, V. Thierry, P. Galaup, C. Coatanoan, and T. Loubrieu (2009), Quality control of large Argo datasets, *J. Atmos. Oceanic Technol.*, *26*, 337–351, doi:10.1175/2008JTECHO552.1.

Glynn, P. W., J. L. Maté, A. C. Baker, and M. O. Calderón (2001), Coral bleaching and mortality in Panama and Ecuador during the 1997–1998 El Niño–Southern Oscillation event: Spatial/temporal patterns and comparisons with the 1982–1983 event, *Bull. Mar. Sci.*, *69*(1), 79–109.

Hayes, S. P., L. J. Mangum, J. Picaut, A. Sumi, and K. Takeuchi (1991), TOGA-TAO: A moored array for real-time measurements in the tropical Pacific Ocean, *Bull. Am. Meteorol. Soc.*, *72*(3), 339–347, doi:10.1175/1520-0477(1991)072<0339:TTAMAF>2.0.CO;2.

Hénin, C., and J. Grelet (1996), A merchant ship thermo-salinograph network in the Pacific Ocean, *Deep Sea Res., Part I*, *43*(11–12), 1833–1855, doi:10.1016/S0967-0637(96)00084-2.

Hénin, C., Y. du Penhoat, and M. Ioualalen (1998), Observations of sea surface salinity in the western Pacific fresh pool: Large-scale changes in 1992–1995, *J. Geophys. Res.*, *103*(C4), 7523–7536, doi:10.1029/97JC01773.

Hofmann, E. E., A. J. Busalacchi, and J. J. O'Brien (1981), Wind generation of the Costa Rica Dome, *Science*, *214*, 552–554, doi:10.1126/science.214.4520.552.

Hsu, P. C., T. Li, and B. Wang (2011), Trends in global monsoon area and precipitation over the past 30 years, *Geophys. Res. Lett.*, *38*, L08701, doi:10.1029/2011GL046893.

Kerr, Y., P. Waldteufel, J. P. Wigneron, J. M. Martinuzzi, J. Font, and M. Berger (2001), Soil moisture retrieval from space: The soil moisture and ocean salinity (SMOS) mission, *IEEE Trans. Geosci. Remote Sens.*, *39*(8), 1729–1735, doi:10.1109/36.942551.

Kessler, W. S. (2002), Mean three-dimensional circulation in the northeastern tropical Pacific, *J. Phys. Oceanogr.*, *32*, 2457–2471, doi:10.1175/1520-0485-32.9.2457.

Kessler, W. S. (2006), The circulation of the eastern tropical Pacific: A review, *Prog. Oceanogr.*, *69*(2–4), 181–217, doi:10.1016/j.pocean.2006.03.009.

Kug, J.-S., F.-F. Jin, and S.-I. An (2009), Two types of El Niño events: Cold tongue El Niño and warm pool El Niño, *J. Clim.*, *22*, 1499–1515, doi:10.1175/2008JCLI2624.1.

Legeckis, R. (1986), A satellite time series of sea surface temperatures in the eastern equatorial Pacific, 1982–1986, *J. Geophys. Res.*, *91*(C11), 12,879–12,886, doi:10.1029/JC091iC11p12879.

Legeckis, R. (1988), Upwelling in the Gulfs of Panama and Papagayo during March 1985, *J. Geophys. Res.*, *93*(C12), 15,485–15,489, doi:10.1029/JC093iC12p15485.

Liang, J.-H., J. C. McWilliams, and N. Gruber (2009), High-frequency response of the ocean to mountain gap winds in the northeastern tropical Pacific, *J. Geophys. Res.*, *114*, C12005, doi:10.1029/2009JC005370.

Linsley, B. K., R. B. Dunbar, G. M. Wellington, and D. A. Mucciarone (1994), A coral-based reconstruction of Intertropical Convergence Zone variability over Central America since 1707, *J. Geophys. Res.*, *99*(C5), 9977–9994, doi:10.1029/94JC00360.

Locarnini, R. A., A. V. Mishonov, J. I. Antonov, T. P. Boyer, H. E. Garcia, O. K. Baranova, M. M. Zweng, and D. R. Johnson (2010), *World Ocean Atlas 2009, vol. 1, Temperature, NOAA Atlas NESDIS*, vol. 68, edited by S. Levitus, 184 pp., NOAA, Silver Spring, Md.

Lukas, R., and E. Lindstrom (1991), The mixed layer of the western equatorial Pacific Ocean, *J. Geophys. Res.*, *96*, 3343–3357.

Lumpkin, R., and Z. Garraffo (2005), Evaluating the decomposition of tropical Atlantic drifter observations, *J. Atmos. Oceanic Technol.*, *22*, 1403–1415, doi:10.1175/JTECH1793.1.

Maes, C. (1998), Estimating the influence of salinity on sea level anomaly in the ocean, *Geophys. Res. Lett.*, *25*(19), 3551–3554, doi:10.1029/98GL02758.

Maes, C. (2008), On the ocean salinity stratification observed at the eastern edge of the equatorial Pacific warm pool, *J. Geophys. Res.*, *113*, C03027, doi:10.1029/2007JC004297.

Maes, C., J. Picaut, and S. Belamari (2002), Salinity barrier layer and onset of El Niño in a Pacific coupled model, *Geophys. Res. Lett.*, *29*(24), 2206, doi:10.1029/2002GL016029.

Maes, C., J. Picaut, and S. Belamari (2005), Importance of salinity barrier layer for the buildup of El Niño, *J. Clim.*, *18*, 104–118, doi:10.1175/JCLI-3214.1.

McPhaden, M. J., M. F. Cronin, and D. C. McClurg (2008), Meridional structure of the seasonally varying mixed layer temperature balance in the eastern tropical Pacific, *J. Clim.*, *21*, 3240–3260, doi:10.1175/2007JCLI2115.1.

Mitchell, T. P., and J. M. Wallace (1992), The annual cycle in equatorial convection and sea surface temperature, *J. Clim.*, *5*, 1140–1156, doi:10.1175/1520-0442(1992)005<1140:TACIEC>2.0.CO;2.

Owens, W. B., and A. P. S. Wong (2009), An improved calibration method for the drift of the conductivity sensor on autonomous CTD profiling floats by θ–S climatology, *Deep Sea Res., Part I*, *56*(3), 450–457, doi:10.1016/j.dsr.2008.09.008.

Pennington, J. T., K. L. Mahoney, V. S. Kuwahara, D. D. Kolber, R. Calienes, and F. P. Chavez (2006), Primary production in the eastern tropical Pacific: A review, *Prog. Oceanogr.*, *69*, 285–317, doi:10.1016/j.pocean.2006.03.012.

Picaut, J., M. Ioualalen, C. Menkes, T. Delcroix, and M. J. McPhaden (1996), Mechanism of the zonal displacements of the Pacific warm pool: Implications for ENSO, *Science*, *274*, 1486–1489, doi:10.1126/science.274.5292.1486.

Poveda, G., and O. J. Mesa (2000), On the existence of Lloró (the rainiest locality on Earth): Enhanced ocean-land-atmosphere interaction by a low-level jet, *Geophys. Res. Lett.*, *27*(11), 1675–1678, doi:10.1029/1999GL006091.

Reul, N., and J. Tenerelli (2011), SMOS Level 3 SSS research products: Product validation document reprocessed year 2010, Tech. Doc. CATDS-CECOS-L3-VALDOC, Inst. Fr. de Rech. Pour l'Exploit. de la Mer, Brest, France. [Available at http://www.ifremer.fr/naiad/salinityremotesensing.ifremer.fr/CATDS_CECOS_SMOS_Level3Products_Validation.pdf.]

Rodriguez-Rubio, E., W. Schneider, and R. Abarca del Rio (2003), On the seasonal circulation within the Panama Bight derived from satellite observations of wind, altimetry and sea surface temperature, *Geophys. Res. Lett.*, *30*(7), 1410, doi:10.1029/2002GL016794.

Roemmich, D., and W. B. Owens (2000), The ARGO project: Global ocean observations for understanding for understanding and prediction of climate variability, *Oceanography*, *13*(2), 45–50.

Schaefer, K. M., and D. W. Fuller (2002), Movements, behavior, and habitat selection of bigeye tuna (Thunnus obesus) in the eastern equatorial Pacific, ascertained through archival tags, *Fish. Bull.*, *100*(4), 765–788.

Sun, F., and J.-Y. Yu (2006), Impacts of Central America gap winds on the SST annual cycle in the eastern Pacific warm pool, *Geophys. Res. Lett.*, *33*, L06710, doi:10.1029/2005GL024700.

Tsuchiya, M., and L. D. Talley (1998), A Pacific hydrographic section at 88°W: Water-property distribution, *J. Geophys. Res.*, *103*, 12,899–12,918, doi:10.1029/97JC03415.

United Nations Educational, Scientific and Cultural Organization (1981), *The Practical Salinity Scale 1978 and the International Equation of State of Seawater 1980*, Tech. Pap. Mar. Sci. 36, 25 pp., Paris.

Vialard, J., and P. Delecluse (1998), An OGCM study for the TOGA decade, part I: Role of salinity in the physics of the western Pacific fresh pool, *J. Phys. Oceanogr.*, *28*, 1071–1088, doi:10.1175/1520-0485(1998)028<1071:AOSFTT>2.0.CO;2.

Wang, B. (1994), On the annual cycle in the tropical eastern central Pacific, *J. Clim.*, *7*, 1926–1942, doi:10.1175/1520-0442(1994)007<1926:OTACIT>2.0.CO;2.

Wooster, W. S. (1969), Equatorial front between Peru and Galapagos, *Deep Sea Res.*, *16*, 407–419.

Wyrtki, K. (1981), An estimate of equatorial upwelling in the Pacific, *J. Phys. Oceanogr.*, *11*, 1205–1214, doi:10.1175/1520-0485(1981)011<1205:AEOEUI>2.0.CO;2.

Xie, S.-P., H. Xu, W. S. Kessler, and M. Nonaka (2005), Air-sea interaction over the eastern Pacific warm pool: Gap winds, thermocline dome, and atmospheric convection, *J. Clim.*, *18*(1), 5–20, doi:10.1175/JCLI-3249.1.

Xu, H., S.-P. Xie, Y. Wang, and R. J. Small (2005), Effects of Central American mountains on the eastern Pacific winter ITCZ and moisture transport, *J. Clim.*, *18*, 3856–3873, doi:10.1175/JCLI3497.1.

Yu, L. (2011), A global relationship between the ocean water cycle and near-surface salinity, *J. Geophys. Res.*, *116*, C10025, doi:10.1029/2010JC006937.

G. Alory, LEGOS, OMP, CNAP, Université de Toulouse, 14 Ave. Edouard Belin, F-31400 Toulouse, France. (gael.alory@legos.obs-mip.fr)

T. Delcroix, S. Illig, and C. Maes, LEGOS, IRD, Université de Toulouse, 14 Ave. Edouard Belin, F-31400 Toulouse, France.

N. Reul, LOS, IFREMER, Technopole de Brest-Iroise, BP 70, F-29280 Plouzané, France.